JOURNAL OF MATERIALS SCIENCE 30 (1995) 1781–1789

Matrix cracking with frictional bridging fibres in continuous fibre ceramic composites

C. H. HSUEH
Metals and Ceramics Division, Oak Ridge National Laboratory, Oak Ridge, TN 37831, USA

Matrix cracking bridged by intact fibres, which debond from the matrix and then slip against the matrix in friction, has been analysed for unidirectional fibre-reinforced ceramic composites under tensile loading parallel to the fibre axis. The effect of bonding at the fibre–matrix interface, Poisson's effect of the fibre, and residual stresses were included in the analysis. Both the crack-opening displacement and the displacement of the composite due to interfacial debonding have been analytically related to the fibre bridging stress. The critical stress for matrix cracking was also analysed. The existing solutions can be recovered by considering a special case in the present generalized solution.

1. Introduction

Ceramic materials exhibit superior performance at high temperatures. However, their utilization in structural components is severely limited by their brittleness. One approach toward substantially reducing this brittleness is by incorporating fibres aligned with the loading direction. The US Department of Energy, Office of Industrial Technologies, has developed a comprehensive strategy and plan for continuous fibre–ceramic composite (CFCC) materials to meet the demands in a variety of industrial applications [1].

The mechanical performance of fibre-reinforced ceramic composites is intimately related to their interfacial properties [2, 3]. To predict the mechanical behaviour of composites, macromechanical modelling has been employed [4–6]. However, theoretical analyses at the micromechanical level are required to define the modules for the macromechanical modelling. A crucial toughening mechanism for the composite involves matrix cracks bridged by intact fibres. These intact fibres debond from and slip against the matrix in friction when the composite is loaded in tension [2, 3]. It is imperative to define a module containing (1) an analytical relation between the fibre bridging stress and other parameters, and (2) the critical stress for matrix cracking. This work has been performed. However, the effects of bonding at the fibre–matrix interface, Poisson's effect of the fibre, and residual stresses are often ignored in the existing analyses [7, 8]. Also, when the fibre bridging stress is related to a displacement, the difference between the crack-opening displacement and the displacement of the composite due to interfacial debonding is not comprehended by many researchers.

The purpose of the present study was to address the issues mentioned above. First, Poisson's effect, interfacial bonding, and residual stresses were included in the analysis. Second, the difference between the crack-opening displacement and the displacement of the composite due to interfacial debonding was addressed, and their analytical relations with the fibre bridging stress were derived. Third, the critical stress for matrix cracking was analysed. Finally, a special case of the present generalized solution has been compared to existing solutions. The present solution can be readily implemented into a macromechanical model (e.g. for the CFCC programme).

2. Analyses

The geometric configuration used in the present analysis is illustrated in Fig. 1, where a remote uniform stress, σ_∞, is applied on a unidirectional composite containing a crack bridged by intact fibres. While the bridging fibres exert a bridging stress, σ_0, to oppose crack-opening, the relative displacement between the fibre and the matrix at the crack surface specifies the crack-opening displacement, $2u_0$. Also, on each loading side of the composite, an additional displacement, u_{debond}, in the loading direction is introduced due to debonding and sliding at the fibre–matrix interface. This problem can be modelled by using a representative volume element (Fig. 2). A fibre with a radius, a, is located at the centre of a coaxial cylindrical shell of the matrix with an outer radius, b, such that a^2/b^2 corresponds to the volume fraction of fibres, V_f (Fig. 2a). At the crack surface, the bridging stress, σ_0, of the fibre can be related to σ_∞ by

$$\sigma_0 = \frac{\sigma_\infty}{V_f} \tag{1}$$

In the absence of interfacial debonding, the composite has a displacement, u_{bonded}, in the axial direction when the fibre is subjected to a loading stress, σ_0 (Fig. 2b). In the presence of interfacial debonding, both the half crack-opening displacement, u_0, and the displacement of the composite due to interfacial debonding, u_{debond}, are shown in Fig. 2c.

0022–2461

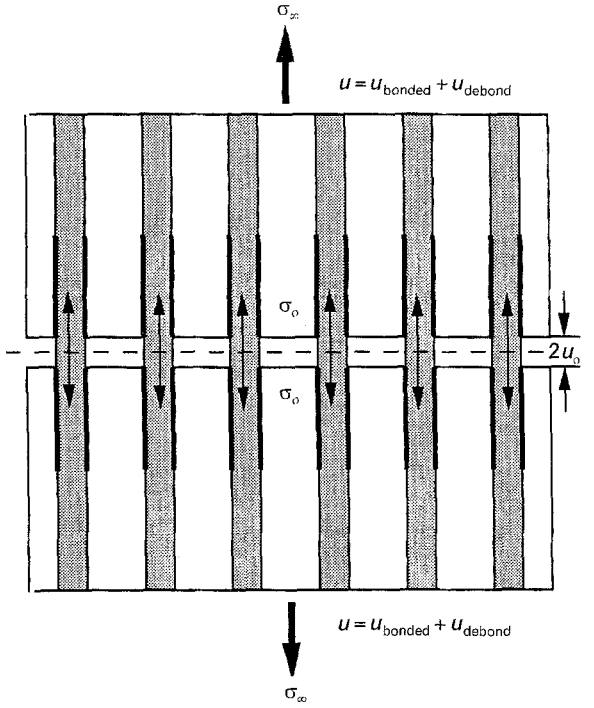

Figure 1 Schematic drawing showing a matrix crack bridged by intact fibres.

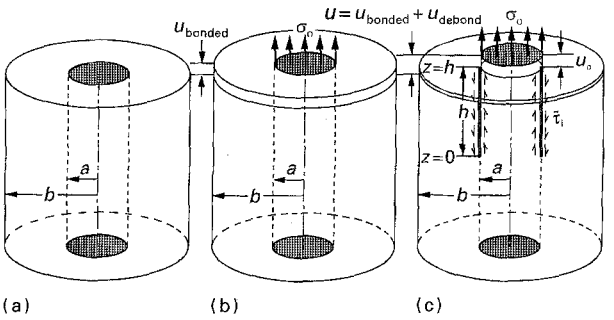

Figure 2 A representative volume element for the fibre bridging problem, (a) prior to loading, (b) loading without interfacial debonding, and (c) loading with interfacial debonding. The half crack opening displacement, u_0, and the displacement of the composite due to interfacial debonding, u_{debond}, are also shown.

When including the three factors (Poisson's effect, interfacial bonding, and residual stresses), the stress analysis for the fibre bridging problem is formidable. When the fibre bridging analysis is incorporated in a macromechanical model, the complexity in the analysis will be compounded. Hence, to facilitate the application of the fibre bridging analysis, a simplified analysis is imperative. Without losing the essence of the three factors, simplifications of the analysis are presented as follows.

2.1. Poisson's effect

The stress transfer from the fibre to the matrix through the interfacial shear stress, τ_i, is dictated by [7–16]

$$\frac{d\sigma_f}{dz} = -\frac{2\tau_i}{a} \tag{2}$$

where σ_f is the axial stress in the fibre, and z is the axial coordinate. When the interface is debonded and subjected to a residual clamping stress, σ_c, the interfacial shear stress dictated by Coulomb friction is [15, 16]

$$\tau_i = \mu(\sigma_c + \sigma_p) \tag{3}$$

where μ is the coefficient of friction, σ_p is the interfacial radial stress induced by Poisson's effect and the loading stress. The residual clamping stress is usually assumed to be constant along the fibre length [13–16]. When Poisson's effect is considered pointwise, the interfacial frictional stress is not constant and the axial stress distribution in the fibre is non-linear due to the non-uniformity of σ_p along the sliding length [13–16] which, in turn, result in the complexity of the analysis. Hence, to simplify the analysis, Poisson's effect along the sliding length is considered not pointwise but in an average sense in the present study. To achieve this, the average value of σ_p (i.e. $\bar{\sigma}_p$) along the sliding length is derived as follows. This averaging technique has been used to analyse the pull-out, push-out and push-in problems, and the results obtained are in excellent agreement with those obtained from rigorous analyses, in which Poisson's effect is considered pointwise [17].

For a frictional interface, the axial stresses in the fibre and the matrix, σ_f and σ_m, vary slowly over distances comparable to the fibre radius. In this case, the characteristics of stresses in any section transverse to the axial direction can be approximated by a Lamé problem, and σ_f and σ_m are approximated to be independent of the radial coordinate [13, 14]. The mechanical equilibrium condition requires

$$V_f\sigma_f + V_m\sigma_m = V_f\sigma_0 \tag{4}$$

where V_m $(= 1 - V_f)$ is the volume fraction of the matrix. The radial and the tangential stresses, σ_r and σ_θ, can be related to σ_p by [13, 14, 18]

$$\sigma_{fr} = \sigma_{f\theta} = \sigma_p \tag{5}$$

for the fibre, and

$$\sigma_{mr} = \sigma_p \qquad \text{at } r = a \tag{6a}$$

$$\sigma_{m\theta} = \frac{-(1 + V_f)\sigma_p}{V_m} \qquad \text{at } r = a \tag{6b}$$

for the matrix at the interface.

The condition that the fibre and the matrix remain in contact during frictional sliding requires continuity of the tangential strain at the interface, such that

$$\frac{1}{E_f}[(1 - \nu_f)\sigma_p - \nu_f\sigma_f] = \frac{1}{E_m} \times \left[-\left(\frac{1 + V_f}{V_m} + \nu_m\right)\sigma_p - \nu_m\sigma_m\right] \tag{7}$$

where E and ν are Young's modulus and Poisson's ratio, and the subscripts, f and m, denote the fibre and the matrix, respectively. Substitution of Equations 4–6

into Equation 7 yields

$$\sigma_p = \left[\left(\frac{\nu_f E_m}{E_f} + \frac{V_f \nu_m}{V_m}\right)\sigma_f - \frac{V_f \nu_m \sigma_0}{V_m}\right] \Big/ D \quad (8)$$

where D is given by

$$D = \frac{1 + V_f}{V_m} + \nu_m + \frac{(1 - \nu_f) E_m}{E_f} \quad (9)$$

Consequently, the solution of $\bar{\sigma}_p$ from Equation 8 is contingent upon the determination of the average value of σ_f (i.e. $\bar{\sigma}_f$) along the sliding length. Replacing σ_p by $\bar{\sigma}_p$ in Equations 2 and 3, the interfacial frictional stress has an average value, $\bar{\tau}_i$, and σ_f varies linearly along the sliding length. However, it is noted that $\bar{\tau}_i$ varies with the sliding zone length and, hence, the loading stress.

The interfacial radial stress due to Poisson's effect, σ_p, is tensile which is greatest at the loaded surface [13–17], counteracts the residual clamping stress, and may result in a frictionless interface. The loading condition satisfying the frictional interface condition (i.e. $\sigma_c + \sigma_p < 0$) is

$$\sigma < -\frac{D E_f}{\nu_f E_m} \sigma_c \quad (10)$$

where σ_c is negative (i.e. compressive). Hence, the present analysis is limited to the loading condition depicted by Equation 10.

2.2. Residual axial stresses

The interface is bonded prior to loading (i.e. no debonding under residual stresses is assumed). The crack surface is traction free, and the residual axial stress is zero at the crack surface. However, the residual axial stresses in the fibre and the matrix increase quickly and reach equilbrium values, σ_{fz} and σ_{mz}, respectively within a length of a few fibre radii underneath the surface [11, 19, 20]. To simplify the present analysis, the residual axial stresses in the fibre and the matrix are assumed to be constants and equal σ_{fz} and σ_{mz}, respectively, along the entire fibre length when the interface remains bonded. Also, to satisfy the mechanical equilibrium condition, σ_{mz} is related to σ_{fz} by

$$\sigma_{mz} = -\frac{V_f \sigma_{fz}}{V_m} \quad (11)$$

Upon interfacial debonding, the residual axial stresses are relaxed which, in turn, induce axial strains $-\sigma_{fz}/E_f$ and $-\sigma_{mz}/E_m$ in the fibre and the matrix, respectively.

2.3. The debonding condition

In the presence of interfacial bonding, an initial debond stress, σ_d, has been defined for the single fibre pull-out problem [15–17]. When the applied stress on the fibre reaches σ_d, interfacial debonding initiates at the loaded surface. During subsequent loading, the debonding zone length, h, increases, and the axial stress in the fibre at the end of the debonding zone is assumed to be equal to σ_d. This is a good assumption for single fibre pull-out where the radial dimension of the specimen is much greater than the fibre radius, and this issue is discussed as follows.

A difference has been noted between debonding at the loaded surface and debonding inside the composite [21]. Whereas the matrix is free at the loaded surface, it is subjected to axial stresses inside the composite due to the stress transfer from the fibre to the matrix. Hence, the magnitude of the interfacial shear stress induced by a loading stress, σ_d, on the fibre at the loaded surface is different from that induced by an axial stress, σ_d, in the fibre inside the composite. However, when the radial dimension of the specimen is much greater than the fibre radius, the axial stress in the matrix is relatively small and the contribution of the matrix axial stress to the interfacial shear is negligible. Hence, it is a good approximation that the axial stress in the fibre is equal to σ_d at the end of the debonding zone for a single fibre pull-out problem. However, during cracking of a composite, multiple fibres are involved in the pull-out process, and the condition that the radial dimension of the surrounding matrix is much greater than the fibre radius is not valid. Hence, modification of the debonding condition is required for the fibre bridging problem in a composite.

The shear stress at the interface results from the tendency of a relative displacement in the axial direction between the fibre and the matrix. It has been proposed that interfacial debonding occurs when the mismatch in the axial strain between the fibre and the matrix reaches a critical value [22, 23]. When the loading stress reaches the debond stress, σ_d, interfacial debonding initiates at the loaded surface, and the critical mismatch strain, ε_d, is

$$\varepsilon_d = \frac{\sigma_d}{E_f} \quad (12)$$

During subsequent loading (i.e. $\sigma_0 > \sigma_d$), interfacial debonding extends underneath the surface, and the mismatch strain at the end of the debonding zone remains ε_d, such that

$$\varepsilon_d = \frac{\sigma_{fd}}{E_f} - \frac{\sigma_{md}}{E_m} \quad (13)$$

where σ_{fd} and σ_{md} are the axial stresses at the end of the debonding zone in the fibre and the matrix, respectively, which satisfy the mechanical equilibrium condition depicted by Equation 4. Combination of Equations 4, 12 and 13 yields

$$\sigma_{fd} = \frac{V_f E_f \sigma_0 + V_m E_m \sigma_d}{E_c} \quad (14a)$$

$$\sigma_{md} = \frac{V_f E_m (\sigma_0 - \sigma_d)}{E_c} \quad (14b)$$

where

$$E_c = V_f E_f + V_m E_m \quad (14c)$$

Equation 14a and b are required in determining the sliding zone length.

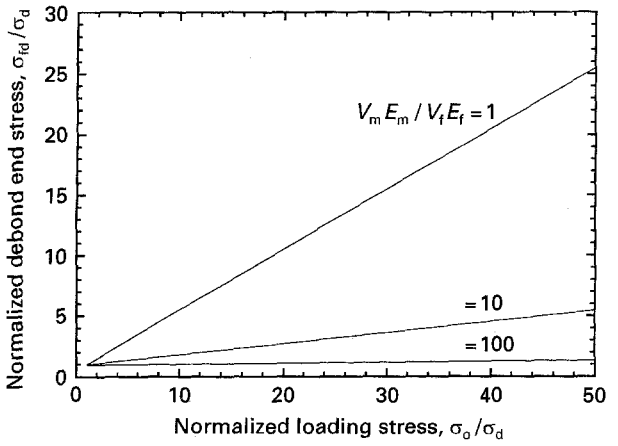

Figure 3 The normalized axial stress in the fibre at the end of the debonded zone, σ_{fd}/σ_d, as a function of the normalized loading stress on the fibre, σ_0/σ_d, at different values of $V_m E_m/V_f E_f$.

It is noted that σ_{fd} and σ_{md} approach σ_d and 0, respectively, when $V_m E_m$ is much greater than $V_f E_f$ (see Equation 14a and b). Hence, the interfacial debonding condition adopted for a single fibre pull-out is valid when $V_m E_m \gg V_f E_f$. To illustrate this, σ_{fd}/σ_d is plotted as a function of σ_0/σ_d at different values of $V_m E_m/V_f E_f$ in Fig. 3. When the applied stress increases, the debonded zone length increases, and the deviation of the axial stress in the fibre at the end of the debonded zone (i.e. σ_{fd}) from the initial debond stress (i.e. σ_d) increases. The slope of the σ_{fd}/σ_d versus σ_0/σ_d curve decreases as $V_m E_m/V_f E_f$ increases.

2.4. The sliding zone length

When Poisson's effect is treated in an average sense, σ_f varies linearly from σ_0 at the loaded end to σ_{fd} at the end of the sliding zone, and $\bar{\sigma}_f$ is

$$\bar{\sigma}_f = \frac{\sigma_0 + \sigma_{fd}}{2} \tag{15}$$

The average value of σ_p along the sliding length can be obtained by substituting σ_f with $\bar{\sigma}_f$ in Equation 8. The corresponding average interfacial frictional stress is

$$\bar{\tau}_i = \mu\left\{\sigma_c + \frac{\left[\left(\frac{\nu_f E_m}{E_f} - \frac{V_f \nu_m}{V_m}\right) + \left(\frac{\nu_f E_m}{E_f} + \frac{V_f \nu_m}{V_m}\right)\frac{V_f E_f}{E_c}\right]\sigma_0 + \left(\frac{\nu_f E_m}{E_f} + \frac{V_f \nu_m}{V_m}\right)\frac{V_m E_m \sigma_d}{E_c}}{2D}\right\} \tag{16}$$

The sign of the shear stress signifies the direction of shear. It is noted that $\bar{\tau}_i$ is negative due to the coordinate system (Fig. 2c) used in the present study, and it is a function of the loading stress (i.e. σ_0) on the fibre.

Adopting the average interfacial frictional stress, the sliding zone length, h, can be obtained from Equation 2, such that

$$h = \frac{-a(\sigma_0 - \sigma_{fd})}{2\bar{\tau}_i} \tag{17a}$$

Substitution of Equation 14a into Equation 17a yields

$$h = \frac{-aV_m E_m(\sigma_0 - \sigma_d)}{2E_c \bar{\tau}_i} \tag{17b}$$

2.5. The displacement

The difference between the crack-opening displacement and the displacement of the composite due to interfacial debonding is not considered by many researchers. This difference is clarified as follows.

2.5.1. The crack-opening displacement

The axial displacement of the fibre at the loaded surface, $w_f(h)$, due to sliding can be obtained by integration of the axial strain along the sliding length, such that

$$w_f = \frac{h(\sigma_0 + \sigma_{fd} - 2\sigma_{fz})}{2E_f}. \tag{18a}$$

The applied stress is in the axial direction, and the axial displacement due to σ_p and Poisson's effect is negligible. Similarly, the axial displacement of the matrix at the loaded surface, $w_m(h)$, is

$$w_m = \frac{h(\sigma_{md} - 2\sigma_{mz})}{2E_m} \tag{18b}$$

The half crack-opening displacement (Fig. 2c), $u_0 (= w_f(h) - w_m(h))$, becomes

$$u_0 = \frac{h}{2E_f}\left(\sigma_0 + \sigma_d - \frac{2E_c\sigma_{fz}}{V_m E_m}\right) \tag{19}$$

2.5.2. The displacement of the composite due to debonding

In the absence of interfacial debonding, the axial strain in the composite, ε_c, is (Fig. 2b)

$$\varepsilon_c = \frac{V_f\sigma_0}{E_c} \tag{20}$$

The corresponding axial displacement, w_c, within a length h is

$$w_c(h) = \frac{hV_f\sigma_0}{E_c} \tag{21}$$

Hence, the additional axial displacement of the composite due to debonding (Fig. 2c), $u_{debond} (= w_f(h) - w_c(h))$, becomes

$$u_{debond} = \frac{h}{2E_f}\left[\frac{V_m E_m(\sigma_0 + \sigma_d)}{E_c} - 2\sigma_{fz}\right] \tag{22}$$

2.6. The matrix cracking stress

The energy-based criterion [7, 8] is adopted to analyse the critical stress required for matrix cracking. For the problem considered in the present study, the following energy terms are involved: (1) $U_{f(a)}$ and $U_{m(a)}$, the elastic strain energies in the fibre and the

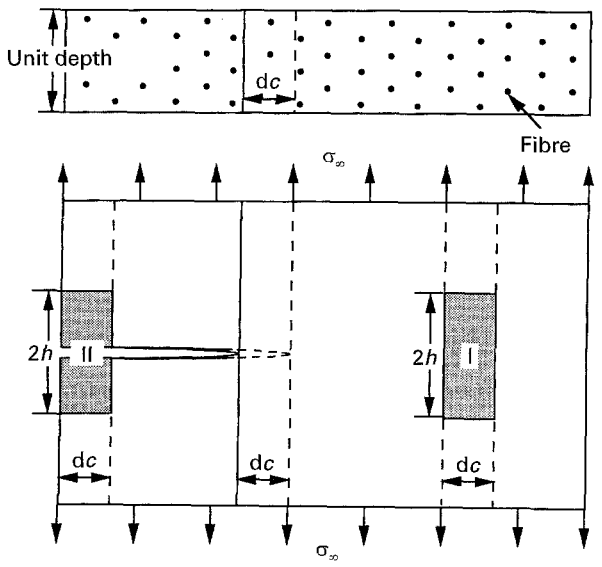

Figure 4 Schematic diagram of a steady-state matrix crack in a long specimen of unit depth to analyse the matrix cracking stress.

matrix which result from the applied stress, (2) $U_{f(r)}$ and $U_{m(r)}$, the elastic strain energies in the fibre and the matrix which result from the residual stresses, (3) U_{int}, the interaction energy between the applied stress and the residual stress, (4) U_s, the energy due to sliding at the debonded interface, (5) G_m, the energy release rate for matrix cracking, (6) G_i, the energy release rate for interfacial debonding, and (7) W, the work done by the applied stress.

To adopt the energy-based cracking criterion, a steady-state matrix crack in a long specimen of unit depth is considered (Fig. 4) [7, 8, 24]. The crack extends through the depth of the specimen with a straight front. Under an applied stress, σ_∞, the crack advances a distance dc. For steady-state cracking, the stress at the crack front remains unchanged during crack extension, and the stresses far behind and ahead of the crack front also remain unchanged. Hence, the energy changes in the specimen due to crack extension are the differences in energy between two strips, which are, respectively, far behind and ahead of the crack front, of thicknesses dc. In the strip far ahead of the crack front, the fibre and the matrix remain bonded. In the strip far behind the crack front, interfacial debonding and sliding occur within a length of $2h$ which is denoted by a shaded region in Fig. 4. Hence, to analyse the energy difference between these two strips, it is sufficient to consider the two shaded regions in Fig. 4 which are designated regions I and II, respectively, for the regions ahead of and behind the crack front.

During crack extension and interfacial debonding, the stress changes in the fibre and the matrix are significant only in the axial direction. Hence, the energy due to only the axial stress is considered for the fibre and the matrix. The solution of the matrix cracking stress is complicated by including the residual axial stress in the analysis. Hence, the residual axial stress is excluded in this section. However, the energy terms due to the residual axial stress, and the effect of the residual axial stress on the matrix cracking stress are shown in the Appendix.

2.6.1. The elastic strain energy in region I due to the applied stress

The fibre and the matrix remain bonded in this region, and the axial strain in the composite is described by Equation 20. The axial stresses in the fibre and the matrix, σ_f and σ_m, are uniform along the axial direction, such that

$$\sigma_f = \frac{V_f E_f \sigma_0}{E_c} \tag{23a}$$

$$\sigma_m = \frac{V_f E_m \sigma_0}{E_c} \tag{23b}$$

The elastic strain energy density in the fibre and the matrix are $\sigma_f^2/2E_f$ and $\sigma_m^2/2E_m$, respectively. With unit depth, the volume in region I is $2h$dc. Because the fibre and the matrix have the volume fractions of V_f and V_m respectively, the corresponding elastic strain energies, $U_{f(a1)}$ and $U_{m(a1)}$, in region I are

$$U_{f(a1)} = \frac{hV_f\sigma_f^2 dc}{E_f} \tag{24a}$$

$$U_{m(a1)} = \frac{hV_m\sigma_m^2 dc}{E_m} \tag{24b}$$

2.6.2. The elastic strain energy in region II due to the applied stress

Interfacial debonding and sliding occur in this region. Adopting the average interfacial frictional stress, the axial stresses in the fibre and the matrix, σ_f and σ_m, are linear along the axial direction, such that

$$\sigma_f = \sigma_{fd} + \frac{z(\sigma_0 - \sigma_{fd})}{h} \quad 0 \leqslant z \leqslant h \tag{25a}$$

$$\sigma_m = \left(1 - \frac{z}{h}\right)\sigma_{md} \quad 0 \leqslant z \leqslant h \tag{25b}$$

In region II, the elastic strain energies in the fibre and the matrix, $U_{f(aII)}$ and $U_{m(aII)}$, are

$$U_{f(aII)} = \frac{V_f dc}{E_f}\int_0^h \sigma_f^2 dz \tag{26a}$$

$$U_{m(aII)} = \frac{V_m dc}{E_m}\int_0^h \sigma_m^2 dz \tag{26b}$$

The elastic strain energy differences between regions II and I are

$$dU_{f(a)} = U_{f(aII)} - U_{f(aI)} \tag{27a}$$

$$dU_{m(a)} = U_{m(aII)} - U_{m(aI)} \tag{27b}$$

Substitution of Equations 14, 17b, 24, and 26 into Equation 27 yields

$$dU_{f(a)} = \frac{-aV_fV_m^2E_m^2(\sigma_0 - \sigma_d)[(3V_fE_f + V_mE_m)(\sigma_0^2 + \sigma_0\sigma_d) + V_mE_m\sigma_d^2]dc}{6\bar{\tau}_iE_fE_c^3} \quad (28a)$$

$$dU_{m(a)} = \frac{aV_f^2V_m^2E_m^2(\sigma_0 - \sigma_d)(2\sigma_0^2 + 2\sigma_0\sigma_d - \sigma_d^2)dc}{6\bar{\tau}_iE_c^3} \quad (28b)$$

2.6.3. The sliding energy and the work

The sliding energy exists in region II but not in region I. In region II, the axial displacements resulted from the axial stresses described by Equations 25a and 25b are

$$w_f(z) = \frac{z[z(\sigma_0 - \sigma_{fd}) + 2h\sigma_{fd}]}{2hE_f} \quad 0 \leqslant z \leqslant h \quad (29a)$$

$$w_m(z) = \frac{z(2h - z)\sigma_{md}}{2hE_m} \quad 0 \leqslant z \leqslant h \quad (29b)$$

Energy is dissipated due to the relative displacement between the fibre and the matrix under a constant interfacial frictional stress, $\bar{\tau}_i$. The sliding energy in region II is equal to the change in the sliding energy due to crack extension, such that

$$dU_s = \frac{-4adc}{b^2}\int_0^h \bar{\tau}_i(w_f - w_m)dz \quad (30a)$$

where the negative sign is due to the negative value of $\bar{\tau}_i$. Substitution of Equations 14, 17b, and 29 into Equation 30a yields

$$dU_s = \frac{-aV_fV_m^2E_m^2(\sigma_0 - \sigma_d)^2(\sigma_0 + 2\sigma_d)dc}{6\bar{\tau}_iE_fE_c^2} \quad (30b)$$

The axial displacement induced by interfacial debonding and resulting from the applied stress can be obtained from Equation 22, such that

$$u_{debond} = \frac{hV_mE_m(\sigma_0 + \sigma_d)}{2E_fE_c} \quad (31)$$

Compared to region I, region II has an additional axial displacement described by Equation 31. With the bridging stress, σ_0, on the fibre, work is done due to this displacement (Equation 31). Hence, the work done due to interfacial debonding is

$$dW = 2V_f\sigma_0u_{debond}dc \quad (32a)$$

Substitution of Equations 17b and 31 into Equation 32a yields

$$dW = \frac{-aV_fV_m^2E_m^2\sigma_0(\sigma_0^2 - \sigma_d^2)dc}{2\bar{\tau}_iE_fE_c^2} \quad (32b)$$

2.6.4. The energy release rates for matrix cracking and interfacial debonding

In region II, the energy required for matrix cracking and interfacial debonding, dG_m and dG_i, are

$$dG_m = V_mG_mdc \quad (33a)$$

$$dG_i = \frac{4ahG_idc}{b^2} \quad (33b)$$

The relation between the energy release rate for interfacial debonding, G_i, and the debond stress, σ_d, has been derived, such that [25, 26]

$$\sigma_d = 2\left(\frac{E_fE_cG_i}{aV_mE_m}\right)^{1/2} \quad (34)$$

Combination of Equations 17b, 33b and 34 gives

$$dG_i = \frac{-aV_fV_m^2E_m^2(\sigma_0 - \sigma_d)\sigma_d^2dc}{2\bar{\tau}_iE_fE_c^2} \quad (35)$$

2.6.5. The matrix cracking stress

The critical stress, which is applied on the fibre, required for matrix cracking, σ_{crit}, can be obtained from the energy balance relation, such that

$$dW = dU_{f(a)} + dU_{m(a)} + dU_s + dG_m + dG_i \quad \text{at } \sigma_0 = \sigma_{crit} \quad (36)$$

Substitution of Equations 28, 30b, 33a, and 35 into Equation 36 yields

$$\sigma_{crit}^3 - 3\sigma_d^2\sigma_{crit} + 2\sigma_d^3 = \frac{-6\bar{\tau}_iE_fE_c^2G_m}{aV_fV_mE_m^2} \quad (37)$$

3. Comparison with existing solutions

Similar problems have been analysed by Aveston *et al.* (ACK) [7] and Marshall *et al.* (MCE) [8]. However, the following conditions were adopted by both the ACK and the MCE models. First, the interface between the fibre and the matrix is assumed to be unbonded. Second, a constant shear stress, τ, is assumed (i.e. Poisson's effect is ignored) within the sliding zone length, h. Third, residual stresses are not considered. The analytical relation between a displacement component and the fibre bridging stress is derived in both models. However, the displacement components in the two models bear different physical meanings. Whereas u_{debond} is considered in the ACK model, u_0 is considered in the MCE model. This difference has not been recognized by many researchers.

In this section, the solutions obtained from the ACK and the MCE models are summarized first. Then, by considering a special case, the present solution is compared to those obtained from these two models. Finally, effects of interfacial bonding and Poisson's effect on the matrix cracking stress are addressed.

3.1. The ACK model [7]

The additional displacement in the fibre due to matrix cracking and interfacial debonding is analysed in the

ACK model, such that

$$u = \frac{aV_m^2 E_m^2 \sigma_0^2}{4E_f E_c^2 \tau} \quad (38)$$

The relative displacement between the fibre and the matrix at the crack surface can also be derived from the ACK model; however, it was not explicitly given. Using the energy balance relation, the critical applied stress on the composite for matrix cracking stress, σ_{crit}^{∞} ($= V_f \sigma_{crit}$), is

$$\sigma_{crit}^{\infty} = \left(\frac{12\tau V_f^2 E_f E_c^2 \gamma_m}{aV_m E_m^2}\right)^{1/3} \quad (39)$$

where γ_m ($= G_m/2$) is the fracture surface energy of the matrix.

3.2. The MCE model [8]

The relative displacement between the fibre and the matrix at the crack surface derived based on the MCE model is

$$u = \frac{aV_m E_m \sigma_0^2}{4E_f E_c \tau} \quad (40)$$

The displacement given by Equation 40 is half the crack-opening displacement.

When Poisson's effect is ignored, $\bar{\tau}_i$ is a constant ($= \mu\sigma_c = -\tau$), Equation 44 becomes identical to that derived in the ACK model (Equation 39), Equation 45 becomes identical to that derived in the MCE model (Equation 40), and Equation 46 becomes identical to that derived in the ACK model (Equation 38). Hence, the existing solutions derived in ACK and MCE models can be recovered by considering a special case in the present generalized solution.

3.4. Effects of interfacial bonding and Poisson's effect on the matrix cracking stress

Both interfacial bonding and the residual axial stress are ignored in the matrix cracking stress defined by Equation 44. When Poisson's effect is also ignored, this matrix cracking stress is redefined as $\sigma_{crit(0)}$.

In the presence of interfacial bonding, the matrix cracking stress, σ_{crit}, can be obtained numerically from Equation 37. Ignoring Poisson's effect, effects of interfaical bonding on the matrix cracking stress are shown in Fig. 5, in which the $\sigma_{crit}/\sigma_{crit(0)}$ ratio is plotted as a function of $\sigma_d/\sigma_{crit(0)}$. The matrix cracking stress increases with the increase in interfacial bonding.

Ignoring interfacial bonding, the $\sigma_{crit}/\sigma_{crit(0)}$ ratio becomes

$$\frac{\sigma_{crit}}{\sigma_{crit(0)}} = \left\{1 + \frac{\left[\left(\frac{\nu_f E_m}{E_f} - \frac{V_f \nu_m}{V_m}\right) + \left(\frac{\nu_f E_m}{E_f} + \frac{V_f \nu_m}{V_m}\right)\frac{V_f E_f}{E_c}\right]\sigma_{crit}}{2D\sigma_c}\right\}^{1/3} \quad (47)$$

3.3. Comparison

In the absence of interfacial bonding and the residual axial stress, Equations 17b, 19, 22, and 37 become

$$h = \frac{-aV_m E_m \sigma_0}{2E_c \bar{\tau}_i} \quad (41)$$

$$u_0 = \frac{h\sigma_0}{2E_f} \quad (42)$$

$$u_{debond} = \frac{hV_m E_m \sigma_0}{2E_f E_c} \quad (43)$$

$$\sigma_{crit} = \left(\frac{-6\bar{\tau}_i E_f E_c^2 G_m}{aV_f V_m E_m^2}\right)^{1/3} \quad (44)$$

Substitution of Equation 41 into Equations 42 and 43 yields

$$u_0 = \frac{-aV_m E_m \sigma_0^2}{4E_f E_c \bar{\tau}_i} \quad (45)$$

$$u_{debond} = \frac{-aV_m^2 E_m^2 \sigma_0^2}{4E_f E_c^2 \bar{\tau}_i} \quad (46)$$

Poisson's effects on the matrix cracking stress are shown in Fig. 6, in which the $\sigma_{crit}/\sigma_{crit(0)}$ ratio is plotted as a function of $-\sigma_c/\sigma_{crit(0)}$ for $\nu_f = \nu_m = 0.3$ and $V_f = 0.3$ at different E_f/E_m ratios. The matrix cracking stress decreases with the decrease in $-\sigma_c/\sigma_{crit(0)}$, and this decrease is more pronounced when E_f/E_m decreases.

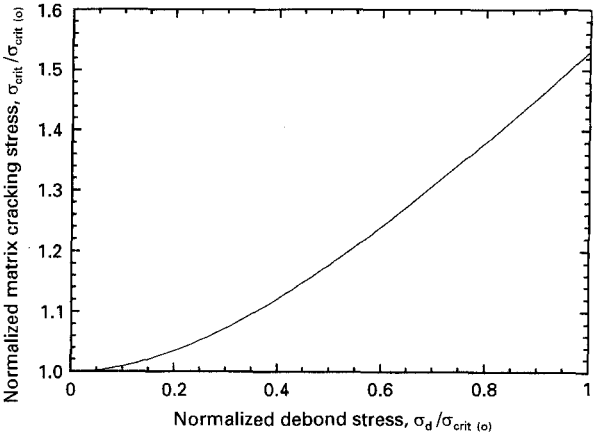

Figure 5 The normalized matrix cracking stress, $\sigma_{crit}/\sigma_{crit(0)}$, as a function of the normalized debond stress, $\sigma_d/\sigma_{crit(0)}$ showing the effects of interfacial bonding on the matrix cracking stress.

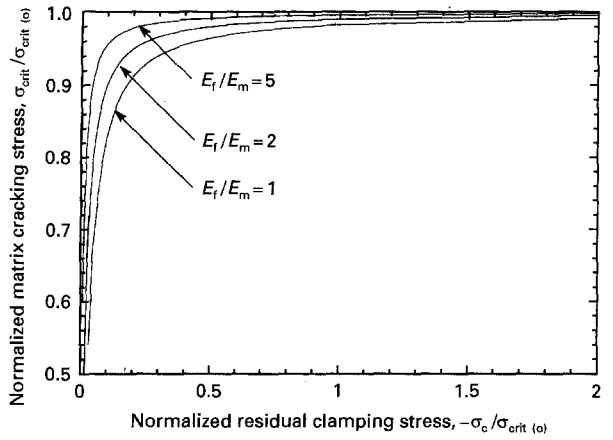

Figure 6 The normalized matrix cracking stress, $\sigma_{crit}/\sigma_{crit(0)}$, as a function of the normalized residual clamping stress, $-\sigma_c/\sigma_{crit(0)}$, for $\nu_f = \nu_m = 0.3$ and $V_f = 0.3$ at different E_f/E_m ratios showing Poisson's effects on the matrix cracking stress.

4. Conclusion

Matrix cracking bridged by intact fibres, which debond from the matrix and then slip against the matrix in friction, has been analysed for unidirectional fibre-reinforced ceramic composites under a tensile loading parallel to the fibre axis. The difference between the crack-opening displacement and the displacement of the composite due to interfacial debonding have been clarified in the present study. Also, the effect of bonding at the fibre–matrix interface, Poisson's effect of the fibre, and residual stresses have been included in the present analysis. The existing solutions can be recovered by ignoring interfacial bonding, Poisson's effect, and residual stresses in the present generalized solution.

The matrix cracking stress increases with the increase in interfacial bonding (Fig. 5). Including Poisson's effect in the analysis, the interfacial frictional stress is decreased [Equation (16)] which, in turn, results in a decrease in the matrix cracking stress (Fig. 6). When the residual axial stress in the matrix is tensile (compressive), the matrix cracking stress is lower (higher) due to the presence of the residual axial stress. To have a better prediction of the mechanical behaviour of fibre-reinforced composite using a macromechanical model, the above three factors should be included in the analysis. The present solution is readily to be implemented into a macromechanical model.

Appendix: Energy due to residual axial stresses

In the presence of residual axial stresses, the elastic strain energy, $U_{f(r)}$ and $U_{m(r)}$, and the interaction energy, U_{int}, exist. These energy terms can be obtained by using Eshelby model [27]. The residual axial stresses result mainly from the mismatch in the stress-free axial strain (e.g. the thermal axial strain) between the fibre and the matrix. To derive the relation between the residual stress and the mismatch in the stress-free strain, the fibre is simulated by an inclusion subjected to a transformation strain ε_T, which is identical to the mismatch in the stress-free strain, in the axial direction.

A.1. The energy in region I

In this region, the fibre and the matrix remain bonded, and continuity of the axial strain is required, such that

$$\frac{\sigma_{fz}}{E_f} + \varepsilon_T = \frac{\sigma_{mz}}{E_m} \tag{A1}$$

where the residual axial stresses, σ_{fz} and σ_{mz}, satisfy the relation described by Equation 11. Combining Equations 11 and A1, the axial transformation strain, ε_T, can be related to σ_{fz} by

$$\varepsilon_T = \frac{-E_c\sigma_{fz}}{V_m E_f E_m} \tag{A2}$$

The total elastic strain energy in the fibre and the matrix is [27]

$$U_{f(rI)} + U_{m(rI)} = -\frac{1}{2}\int \sigma_{fz}\varepsilon_T dV \tag{A3}$$

where V is the volume of the fibre. Hence, the total elastic strain energy in region I is

$$U_{f(rI)} + U_{m(rI)} = -hV_f\sigma_{fz}\varepsilon_T dc \tag{A4}$$

The interaction energy of the residual axial stress with the applied stress is [27]

$$U_{int(I)} = -\int \sigma_f \varepsilon_T dV \tag{A5}$$

where σ_f is uniform along the fibre length and is defined by Equation (23a). The total interaction energy in region I is

$$U_{int(I)} = \frac{-2hV_f^2 E_f \sigma_0 \varepsilon_T dc}{E_c} \tag{A6}$$

A.2. The energy in region II

In this region, the residual axial stresses are completely relaxed due to interfacial debonding, and the total elastic strain energy in the fibre and the matrix is zero, i.e.

$$U_{f(rII)} + U_{m(rII)} = 0 \tag{A7}$$

The interaction energy of the residual axial stress with the applied stress is dictated by Equation A5. However, the axial stress in the fibre, σ_f, is described by Equation 25a. Hence, in region II, the total interaction energy in the fibre and the matrix is

$$U_{int(II)} = -2V_f dc \int_0^h \left[\sigma_{fd} + \frac{z(\sigma_0 - \sigma_{fd})}{h}\right]\varepsilon_T dV \tag{A8}$$

A.3. The contribution of the residual axial stress to the energy change during matrix cracking

The contribution of the residual axial stress to the energy change during matrix cracking is

$$dU_{f(r)} + dU_{m(r)} + dU_{int} = U_{f(rII)} + U_{m(rII)} - U_{f(rI)} - U_{m(rI)} + U_{int(II)} - U_{int(I)} \tag{A9}$$

Subsitution of Equations 14a, 17b, A4, A6, A7 and A8 into Equation A9 yields

$$dU_{f(r)} + dU_{m(r)} + dU_{int} = \frac{-aV_f(\sigma_0 - \sigma_d)dc}{2\bar{\tau}_i E_f} \times \left[\frac{V_m E_m(\sigma_0 + \sigma_d)}{E_c} - \sigma_{fz}\right]\sigma_{fz} \quad \text{(A10)}$$

In the presence of residual axial stresses, the energy balance equation (Equation 36) is replaced by

$$dW = dU_{f(a)} + dU_{m(a)} + dU_{f(r)} + dU_{m(r)} + dU_{int} + dU_s + dG_m + dG_i \quad \text{at } \sigma_0 = \sigma_{crit} \quad \text{(A11)}$$

When the residual axial stress in the fibre is tensile (i.e. $\sigma_{fz} > 0$), the corresponding residual axial stress in the matrix is compressive, and the contribution of residual axial stresses to the energy change during matrix cracking (i.e. Equation A10) is positive. To satisfy Equation A11 for matrix cracking, more work and, hence, higher applied stress is required. Conversely, when residual axial stresses in the fibre and the matrix are compressive and tensile, respectively, the matrix cracking stress is lower due to the presence of residual axial stresses.

Acknowledgements

The author thanks Dr P. F. Becher, Professor Y. Weitsman, and Dr E. Lara-Curzio for reviewing the manuscript. The research was jointly sponsored by the US Department of Energy, Division of Materials Sciences, and Assistant Secretary for Conservation and Renewable Energy, Office of Industrial Technologies, Industrial Energy Efficiency Division, under contract DE-AC05-84OR21400 with Martin Marietta Energy Systems, Inc.

References

1. M. A. KARNITZ, D. F. CRAIG and S. L. RICHLEN, *Ceram. Bull.* **70** (1991) 430.
2. A. G. EVANS and R. M. McMEEKING, *Acta Metall.* **34** (1986) 2435.
3. P. F. BECHER, C. H. HSUEH, P. ANGELINI and T. N. TIEGS, *J. Am. Ceram. Soc.* **71** (1988) 1050.
4. Y. WEITSMAN and H. ZHU, *J. Mech. Phys. Solids* **41** (1993) 351.
5. P. PLUVINAGE and J. M. QUENISSET, *J. Compos. Mater.* **27** (1993) 152.
6. J. KIBLER, in "Continuous Fiber Ceramic Composites Program Task 2", edited by M. Harris, R. A. Lowden and M. A. Karnitz, Bimonthly Progress Report for June-July 1993.
7. J. AVESTON, G. A. COOPER and A. KELLY, "The Properties of Fibre Composites", Conference Proceedings, National Physical Laboratory, Guildford (IPC Science and Technology Press, 1971) pp. 15–26.
8. D. B. MARSHALL, B. N. COX and A. G. EVANS, *Acta Metall.* **33** (1985) 2013.
9. A. TAKAKU and R. G. C. ARRIDGE, *J. Phys. D Appl. Phys.* **6** (1973) 2038.
10. H. STANG and S. P. SHAH, *J. Mater. Sci.* **21** (1986) 953.
11. L. N. McCARTNEY, *Proc. R. Soc. Lond.* **A425** (1989) 215.
12. C. H. HSUEH, *Acta Metall. Mater.* **38** (1990) 403.
13. Y. C. GAO, Y. W. MAI and B. COTTERELL, *J. Appl. Math. Phys.* **39** (1988) 550.
14. J. W. HUTCHINSON and H. M. JENSEN, *Mech. Mater.* **9** (1990) 139.
15. C. H. HSUEH, *Mater. Sci Eng.* **A145** (1991) 135.
16. *Idem, ibid.* **A145** (1991) 143.
17. *Idem, ibid.* **A161** (1993) L1.
18. S. P. TIMOSHENKO and J. N. GOODIER, "Theory of Elasticity" (McGraw-Hill, New York, 1951) p. 70.
19. R. MUKI and E. STERNBERG, *Int. J. Solids Struct.* **6** (1970) 69.
20. C. H. HSUEH, *J. Mater. Sci. Lett.* **7** (1988) 497.
21. J. K. KIM, C. BAILLIE and Y. W. MAI, *J. Mater. Sci.* **27** (1992) 3143.
22. N. SHAFRY, D. G. BRANDON and M. TERASAKI, *Euro-Ceram.* **3** (1989) 3.453.
23. Y. KAGAWA and K. HONDA, *Ceram. Eng. Sci. Proc.* **12** (1991) 1127.
24. B. BUDIANSKY, J. W. HUTCHINSON and A. G. EVANS, *J. Mech. Phys. Solids* **34** (1986) 167.
25. P. G. CHARALAMBIDES and A. G. EVANS, *J. Am. Ceram. Soc.* **72** (1989) 746.
26. C. H. HSUEH, *Mater. Sci. Eng.* **A159** (1992) 65.
27. J. D. ESHELBY, *Proc. R. Soc.* **A241** (1957) 376.

Received 7 January
and accepted 4 October 1994